Available online at www.sciencedirect.com
SCIENCE DIRECT®
International Journal of Multiphase Flow 31 (2005) 141–154
International Journal of Multiphase Flow
www.elsevier.com/locate/ijmulflow

Optical fibre probe measurements of bubbly flow in hydraulic jumps

F. Murzyn *, D. Mouaze, J.R. Chaplin

School of Civil Engineering and the Environment, University of Southampton, Faraday Building, Highfield, Southampton SO17 1BJ, UK

Received 18 December 2003; received in revised form 7 September 2004

Abstract

This paper describes measurements of void fractions, bubble frequencies and bubble sizes in hydraulic jumps with Froude numbers 2.0, 2.4, 3.7 and 4.8. In each case data were obtained with a dual-tip optical fibre probe at a large number of points throughout the jump. Across the lower part of the flow, dominated by air entrainment into a region of turbulent shear, void fractions follow a Gaussian distribution. In the upper region, dominated by interactions with the free surface, the void fraction follows the form of an error function. The intersection between these two profiles provides a well-defined boundary between the two regions. Comparisons are made with measurements at higher Froude numbers [by Chanson, H., Brattberg, T., 2000. Experimental study of the air–water shear flow in a hydraulic jump. International Journal of Multiphase Flow 26, 583–607] revealing a very large measure of compatibility between the two sets of data.

Keywords: Hydraulic jump; Two-phase flow; Void fraction; Bubble frequency; Sauter mean diameter; Optical fibre probe; Dual-tip probe

* Corresponding author. Fax: +33 (0)1 60 957297.
E-mail address: frederic.murzyn@univ-mlv.fr (F. Murzyn).

0301-9322/$ - see front matter © 2004 Published by Elsevier Ltd.
doi:10.1016/j.ijmultiphaseflow.2004.09.004

1. Introduction

The hydraulic jump is an example of the interaction of strong turbulence with a free surface. For the purposes of studying experimentally such flows in detail it is a convenient case, because it is simple to set up in the laboratory and because its bulk stationary properties are primarily determined by a single parameter, the Froude number. As with all flows involving interactions at an interface, it is true that the physics, chemistry and biology of the surface can also have major effects on some characteristics of the motion. The difference between breaking waves in freshwater and seawater provides a very clear example of some of these effects (Wu, 2000). Another relevant factor is the extent to which the channel flow upstream of the jump is fully developed, a distinction discussed by Resch et al. (1976). Nevertheless, under laboratory conditions with clean freshwater the hydraulic jump represents a simply-defined problem that can be used as a vehicle for advancing our understanding of mechanisms that are present not only in breaking waves of various kinds (where it is responsible for air/sea exchanges of climatic importance), but in plunging jets, self-aerating channel flows and discharges into the atmosphere.

Recent measurements in hydraulic jumps include those of Waniewski (2001) using phase Doppler anemometry, and Liu et al. (2002) who used Acoustic Doppler Velocimetry. The presence of large quantities of air in the flow (either in the form of bubbles or as a result of large and high frequency deformations of the surface) ultimately generates severe practical problems for non-intrusive optical and acoustic techniques. Another strand of research has concentrated on identifying the distribution of air in the hydraulic jump, and it is this approach which is the focus of the present paper. In this field a major contribution has been made by Chanson and his colleagues, not only in the hydraulic jump (Chanson and Qiao, 1994; Chanson and Brattberg, 1997), but in other aerated flows including those in open channels (Chanson, 1997), water jets in free fall (Brattberg et al., 1998) and plunging jets (Chanson and Manasseh, 2003).

A review of the other (rather limited) literature on air content measurements in hydraulic jumps, and a consolidation of the results, is provided by Chanson and Brattberg (2000). Most of these have been made with single or double conductivity probes which rely on the considerable difference between the electrical resistivities of air and water to distinguish the two phases. Double probes record the presence of air or water at two points in close proximity, and from the results one can infer the component of velocity of the bubbles in the direction of a line joining the two probes, and a measure of their size. The external stainless steel electrodes of the pointed double probes used by Chanson and Brattberg (1997) were 200 μm in diameter, and their signals were sampled at a rate of up to 20 kHz. A review of experimental techniques in gas–liquid flows is presented by Boyer et al. (2002) where intrusive and non-intrusive techniques are discussed as well as analysis methods.

In the experiments described in the present paper we used optical phase-detection probes, which rely on the difference between the refractive indices of air and water. The principle of this instrument, in which an individual probe contains an optical fibre, is described and discussed in Cartellier and Achard (1990), Cartellier and Barrau (1998) and Boyer et al. (2002). Changes in the intensity of light reflected from the immersed end of the fibre by the passage of an air/water interface are detected by an optical amplifier at the other end. Using this technique with a double probe, we made measurements in hydraulic jumps at Froude numbers between 2.0 and 4.8.

The aim was to explore the two-phase properties of flows that had not been previously studied in this way, and compare the results with those of Chanson and Brattberg (1997), cited in Chanson and Brattberg (2000). Though the Froude numbers in their experiments were higher (6.3 and 8.5) it was possible for the most part to present both sets of data in a unified way, which revealed both the structure of the flow and a strong measure of agreement (and some discrepancies) on void fractions, bubble frequencies and Sauter mean diameters. We were able to identify a clear boundary between the upper re-circulating region, in which air entrainment is dominated by aeration at the upper surface, and the lower turbulent shear region which has a steady supply of air bubbles from the foot [1] of the jump.

2. Experimental arrangements and flow conditions

The experiments were performed in a 12 m long horizontal re-circulating glass-sided channel at the University of Southampton. The channel cross section is 0.3 m wide and 0.4 m high, and it has a flat bottom with a measured surface roughness of $k_s = 0.3$ mm.

The hydraulic jump was formed a short distance downstream from a sluice gate, about 7 m from the weir at the downstream end of the channel. Good control on the flow rate ensured that the position of the jump was almost stationary, but to improve its stability further a 10 mm square bar was placed across the floor of the channel 1.2 m downstream of its foot. After each change of conditions, several minutes were allowed to elapse before any measurements were made. The aperture beneath the sluice gate, which was between 0.28 m and 0.36 m upstream of the foot of the jump (see Table 1), was set at between 0.03 m and 0.09 m. The channel forms part of a re-circulating system which incorporates a large reservoir, and there were no bubbles in the incident flow.

The origin of the reference frame (x, z) is on the bottom of the channel directly beneath the foot of the hydraulic jump (see Fig. 1) where the incoming flow has a depth h. At this point and elsewhere, water depths were measured with a miniature resistive wire gauge (Mouaze et al., 2004) comprising two parallel 50 μm vertical wires separated by 1 mm. This gauge has a resolution of much less than 1 mm, and provides a linear output. Estimates of the bed boundary layer at the foot of the jump suggest thicknesses between $0.18h$ and $0.36h$, and no free surface aeration took place upstream of this point. The inflow conditions at the hydraulic jump can therefore be considered as partially-developed. The incident velocity U just upstream of the foot of the jump and the Froude number $Fr = U/\sqrt{gh}$ were estimated from measurements of h and the depth of flow h_d far downstream of the jump.

Measurements inside the jump were made with an RBI dual-tip probe optical phase-detection instrument. This used the technique described by Cartellier and Achard (1990), to signal the presence of air or water at the ends of each of two parallel 10 μm diameter optical fibres, 1 mm apart. The fibres extend 5 mm beyond the ends of 25 mm long, 0.8 mm diameter cylindrical

[1] Most authors refer to the upstream edge of the hydraulic jump as its "toe". Following Brocchini and Peregrine (2001), we prefer to call this point the "foot" so that the term "toes" can in future be used to identify the (unsteady) irregularities in the upstream limit of the jump when viewed from above.

Table 1
Experimental conditions, with values of the water depth h and velocity U just upstream of the foot, and the water depth h_d downstream of the jump

Test	h (m)	h_d (m)	U (m/s)	Fr	Distance sluice gate to foot (m)	x/h
a	0.059	0.138	1.50	2.0	0.36	0.85 1.70 2.54 4.24
b	0.046	0.137	1.64	2.4	0.28	2.17 4.35 6.52 8.70 10.9
c	0.032	0.150	2.05	3.7	0.34	4.69 7.81 15.6 20.3 25.0
d	0.021	0.133	2.19	4.8	0.36	7.14 11.9 23.8 31.0 38.1

Streamwise positions at which the measurements were made are given in terms of x/h, where x is measured from the foot.

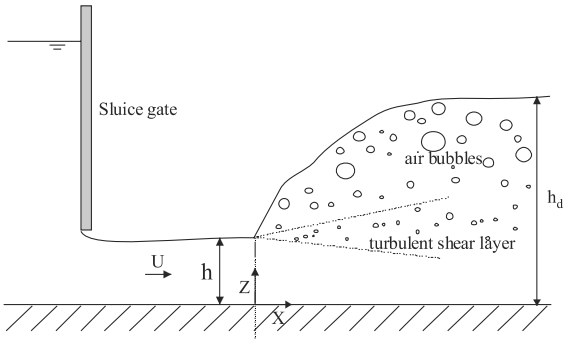

Fig. 1. Definition sketch.

supports which are connected to a 2.5 m diameter mounting rod as shown in Fig. 2. The settling time of each channel, determined by the response of the probe, the optical amplifier and the output circuitry, is less than 1 μs. Data from each fibre was sampled at a rate of up to 1 MHz, to provide measurements of the void fraction as well as bubble frequencies, velocities and chord lengths, from which a characteristic bubble diameter can be inferred as described below. In a slow moving flow the smallest detectable bubble is of a size comparable to the 10 μm diameter of the optical fibres, but at higher velocities the limiting size becomes a function of the settling time and data acquisition frequency. Photographs of the flow showed the vast majority of bubbles to be much larger than 1 mm, so that the passage of each bubble would be recorded by several hundred data points. There is no upper limit to the size of bubbles that could be detected. The probe tips were aligned so that they were at the same elevation above the bed of the channel, one directly downstream of the other. The Reynolds number associated with the flow past each probe was less than 30, and at a separation of 100 diameters it seems reasonable to assume that the effect of the upstream probe on the downstream one would be negligible. The probes were placed in turn at a large number of positions throughout the jumps, and at each point data was always collected during 2 min, which was found to be sufficient to ensure stable results.

Four sets of experiments are presented in this paper, characterized by four different Froude numbers as set out in Table 1. For each position x/h, the vertical step between measurement points was 5 mm in the lower part of the flow, reducing to 2 mm in the upper part.

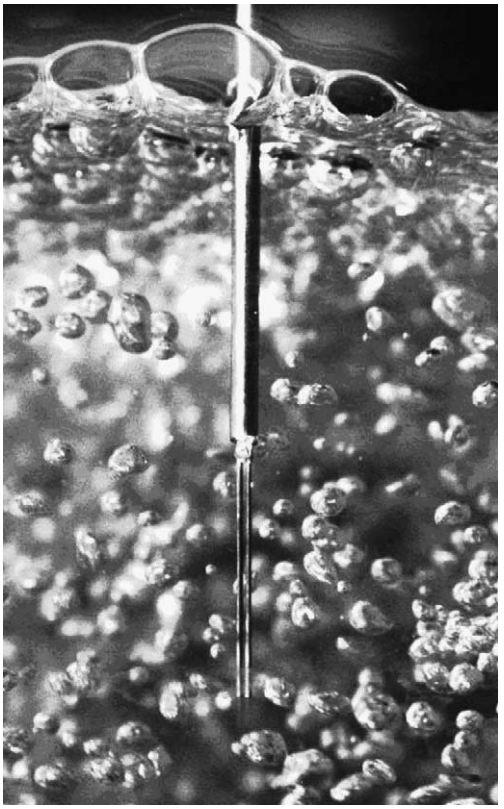

Fig. 2. The RBI dual-tip probe. The length of the 0.8 mm diameter parallel supports is 25 mm. The optical fibres (not visible) extend a further 5 mm.

3. Results and discussion

3.1. Void fractions

Air enters the hydraulic jump at the foot to provide a steady source of bubbles which disperse and are convected downstream in the turbulent flow. Fig. 3 shows the dispersion of bubbles at $Fr = 3.0$, and the bubbly mixture further downstream at $Fr = 5.0$. In the region of the turbulent shear layer (see Fig. 1) and below, the mean flow velocity was considerably greater than the bubble rise velocity, about 0.3 m/s for bubbles in the range of sizes 1 mm–5 mm (Clift et al., 1978). In this lower region it is argued by Chanson (1996) that the void fraction C (representing the proportion of the measurement period during which air is detected at the measurement point) should satisfy a diffusion equation of the form

$$u\frac{\partial C}{\partial x} + C\frac{\partial u}{\partial x} = \frac{\partial}{\partial z}\left(D\frac{\partial C}{\partial z}\right), \tag{1}$$

where u is a representative horizontal velocity and D a diffusion coefficient. On a given vertical plane x this suggests a void fraction profile of the form

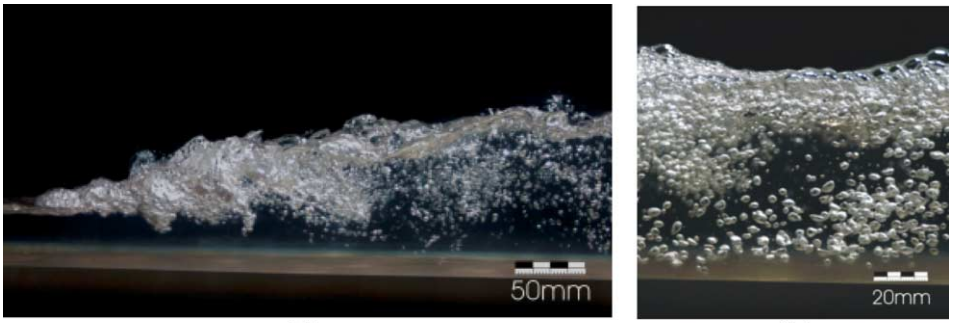

Fig. 3. Hydraulic jumps at (a) $Fr = 3.0$, and (b) $Fr = 5.0$ at 0.25 m from the foot.

$$C = C_{\max} \exp\left(-\frac{1}{4}\frac{U}{D}\frac{(z - z_{C\max})^2}{x}\right), \tag{2}$$

where C reaches a maximum $C_{\max}$ at the point $(x, z_{C\max})$.

The air content in the upper part of the hydraulic jump on the other hand is at least initially dominated by interfacial aeration at the free surface. Similar conditions exist at the edge of water jets freely discharging into air, a situation in which Brattberg et al. (1998) found that the void fraction followed the form.

$$C = \frac{1}{2}\left[1 + \operatorname{erf}\left(\frac{z - z_{C50}}{2\sqrt{Dx/U}}\right)\right], \tag{3}$$

also a solution of an appropriate diffusion equation. In this profile, $C = 1/2$ at $z = z_{C50}$, and $C \to 1$ as $z \to \infty$.

A typical set of measurements of the void fraction are shown in Fig. 4(a). The void fraction is plotted against the elevation z for constant x. Two distinct regions can be clearly identified. In the

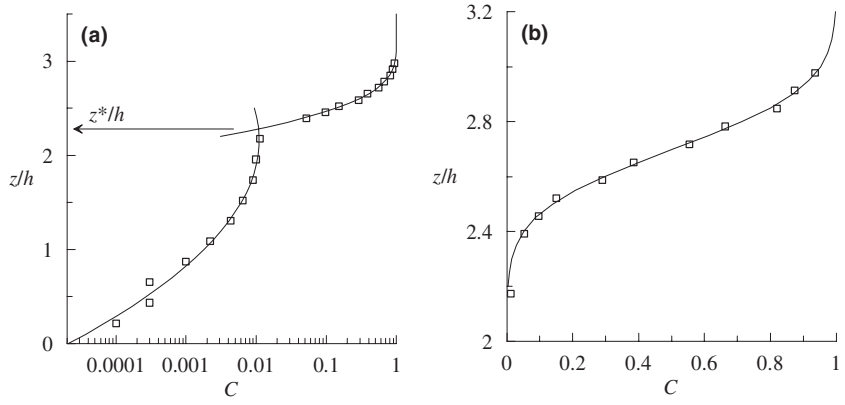

Fig. 4. Typical void fraction distributions; $Fr = 2.4$, $x/h = 8.7$. The measurements are shown as points, to which profiles of the form of Eq. (2) (in the lower region) and Eq. (3) (in the upper region) are fitted. Data for the upper region are re-plotted with a linear scale on the right. The intersection between the two fitted lines defines an elevation z^*.

lower region the measured void fractions are fitted to, and follow, a relationship of the form of Eq. (2), while in the upper region they can be seen to be a close match to that of Eq. (3). The same data are plotted in Fig. 4(a) and (b) on different scales, demonstrating very good agreement with the characteristic profiles in both regions. The intersection between the two profiles defines an elevation z^*.

In Figs. 5 and 6 are plotted all void fraction measurements for all available values of x, for six Froude numbers. Four of these ($Fr = 2.0$, 2.4, 3.6 and 4.8) were from the present measurements, while the data for the others (also discussed below, at $Fr = 6.3$ and 8.5) are taken from Chanson and Brattberg (1997, 2000). The data are normalised in ways suggested by Eqs. (2) and (3) respectively and show excellent agreement with those profiles in their respective regions. At the top of the lower region (Fig. 5) and at the bottom of the upper region (Fig. 6) the data systematically break away from the plotted trends as the transition between the two zones is approached.

In each of these cases, values of $C_{\max}$, $z_{C\max}$, z_{C50}, z^* and D were obtained by fitting the data to the appropriate profiles. The results obtained for these parameters are plotted in Figs. 7 and 8. Lines drawn for each Froude number in Fig. 7(a) are of the form $C_{\max} \propto \exp(-Ax)$, and it is seen that all the data match this behaviour rather better than that of a power law suggested by Chanson and Brattberg (2000). On the other hand $z_{C\max}$ appears to be initially proportional to x as shown by a line in Fig. 7(b) with a gradient (derived for all the data in this range) of 0.102, in close agreement with their figure of 0.108. The diffusion coefficients plotted in Fig. 7(c) are rather scattered, though dashed lines through the present data suggests some structure different from that in Chanson and Brattberg's results.

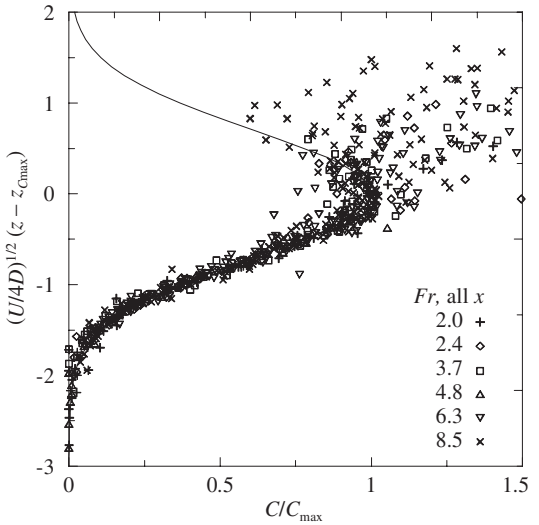

Fig. 5. Void fractions plotted against elevations normalised in accordance with Eq. (2) which is shown as a continuous line. For each Froude number the data points cover all available values of x/h. For Froude numbers up to 4.8 these are set out in Table 1. All data for Froude numbers 6.3 and 8.5 are from Chanson and Brattberg (1997). At $Fr = 6.3$ their measurements were made at $x/h = 3.57$, 7.14, 10.7, 14.3, 21.4, 28.6, 35.7; at $Fr = 8.5$, at $x/h = 1.43$, 3.57, 7.14, 10.7, 14.3, 21.4, 28.6, 39.3, 50.0.

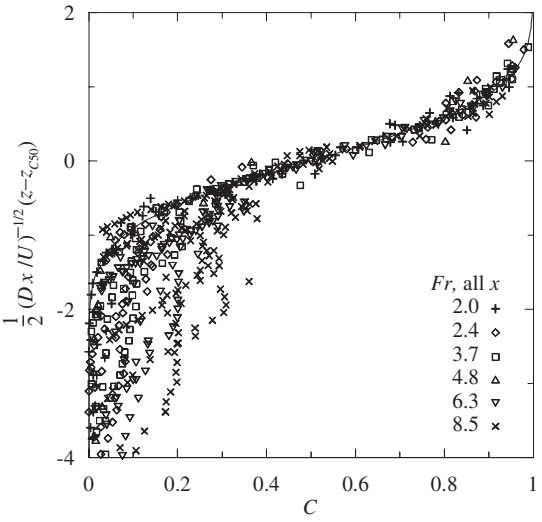

Fig. 6. Void fractions plotted against elevations normalised in accordance with Eq. (3) which is shown as a continuous line. For each Froude number the data points cover all available values of x/h. For Froude numbers up to 4.8 these are set out in Table 1. All data for Froude numbers 6.3 and 8.5 are from Chanson and Brattberg (1997). At $Fr = 6.3$ their measurements were made at $x/h = 3.57$, 7.14, 10.7, 14.3, 21.4, 28.6, 35.7; at $Fr = 8.5$, at $x/h = 1.43$, 3.57, 7.14, 10.7, 14.3, 21.4, 28.6, 39.3, 50.0.

Fig. 8 shows the elevations z_{C95} (at which $C = 0.95$), z_{C50} and z^* (plotted on the same scales), and the diffusion coefficient D relating to the upper layer. Continuous lines in Fig. 8(a)–(c) represent the mean initial rates of increase in z_{C95}, z_{C50} and z^* with x (0.37, 0.26 and 0.19 respectively), showing how the region predominantly influenced by interfacial aeration initially increases in thickness with distance downstream from the foot of the jump. Further downstream these measures converge as the void ratio diminishes and the surface becomes calmer. Also the diffusion coefficient (Fig. 8(d)) in the upper layer decays faster than that in the lower layer (Fig. 7(c)).

3.2. Bubble frequencies

Another characteristic of the flow that was monitored with the optical probes is the bubble encounter frequency F. Bubble frequencies are plotted in Fig. 9 in the normalised form Fh/U for four Froude numbers. Three of these refer to our measurements, the fourth to those of Chanson and Brattberg (1997). The elevation z is scaled to z_{C95} which is a convenient measure of the elevation of the water surface at the top of the jump. Continuous lines in Fig. 9 refer to the region $z < z^*$, where the bubble frequencies reach a maximum approximately in accordance with the observation by Chanson and Brattberg that here F is correlated with C. Broken lines denote the region where $z > z^*$.

Near $z \sim z_{C95}$ the frequency profiles at all sections follow a similar behaviour with F diminishing at an almost uniform rate towards zero. In this region the observed frequency reflects the structure of the air/water interface of the top of the jump rather than the passage of air bubbles, and it can be seen that in most cases there is a maximum perceived bubble frequency in this zone as well as a second maximum within the turbulent shear layer.

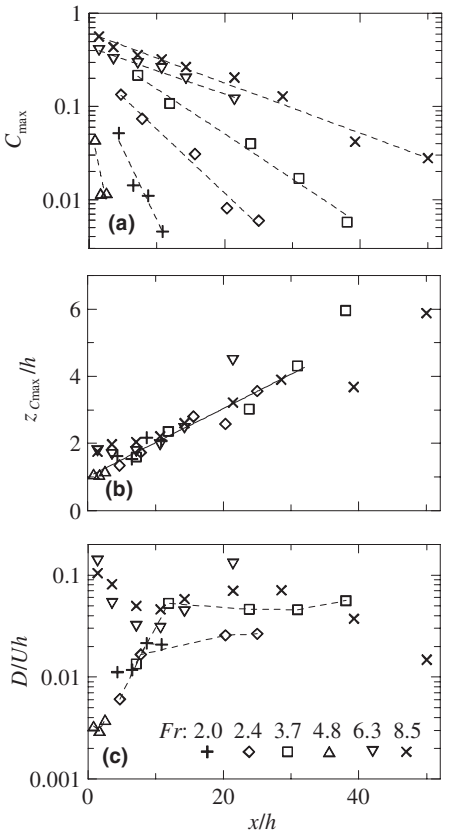

Fig. 7. Parameters for the lower region obtained by fitting Eq. (2) to the measurements; (a) maximum void fraction; (b) the elevation corresponding to the maximum void fraction; (c) the diffusion coefficient. Data for $Fr = 6.3$ and 8.5 are from Chanson and Brattberg (1997).

Maximum normalised frequencies within the region $z < z^*$ on each cross section are plotted as a function of distance downstream from the foot in Fig. 10. There is a measure of agreement with the corresponding results of Chanson and Brattberg (where maximum measured bubble frequencies were well over 100 Hz) though in the latter there is initially less variation with x.

3.3. Bubble sizes

Bubble sizes can be characterised in terms of the Sauter mean diameter d_s (Clift et al., 1978). This is the diameter of the bubble whose volume/surface ratio is the same as that calculated for all bubbles observed during the test. For present purposes the Sauter mean diameter is given by

$$d_s = \frac{3Cu}{2F}, \tag{4}$$

where u is the mean bubble velocity which in our case was obtained directly from the dual-tip optical probes.

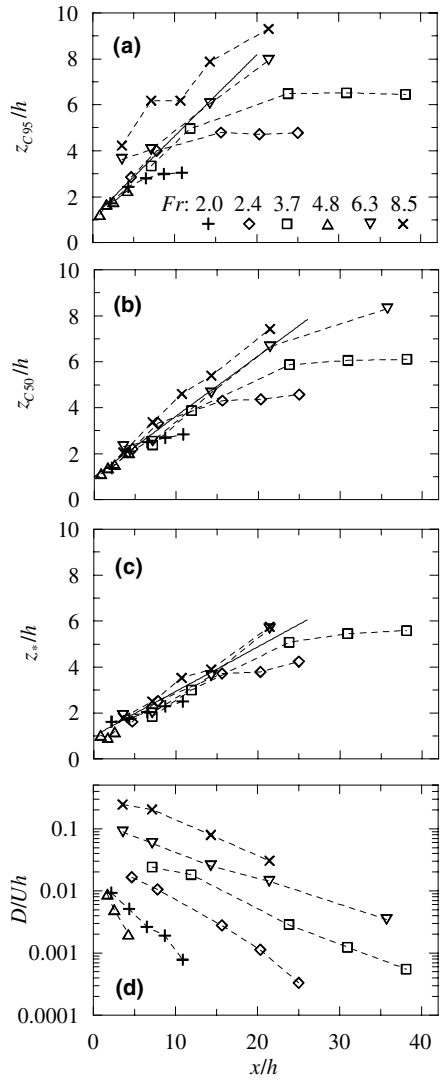

Fig. 8. Parameters for the upper region obtained by fitting Eq. (3) to the measurements; (a) the elevation at which the void fraction is 95%; (b) the elevation at which the void fraction is 50%; (c) the elevation of the intersection between the two profiles; (d) the diffusion coefficient. Data for $Fr = 6.3$ and 8.5 are from Chanson and Brattberg (1997). Continuous lines in (b) and (c) are best linear fits to all data.

The distribution of Sauter mean diameters over the vertical was found to be remarkably similar at all Froude numbers and over a wide range of positions along the channel. Typical results are plotted in Fig. 11 for the region in which $C < 0.25$ (since the concept of bubble diameter can have little meaning for larger void ratios). Comparable data inferred from Chanson and Brattberg's measurements of C, u and F, shown in Fig. 11(d), are more scattered but follow a similar trend. In all cases the data points are joined with continuous lines in the region $z < z^*$ and broken lines

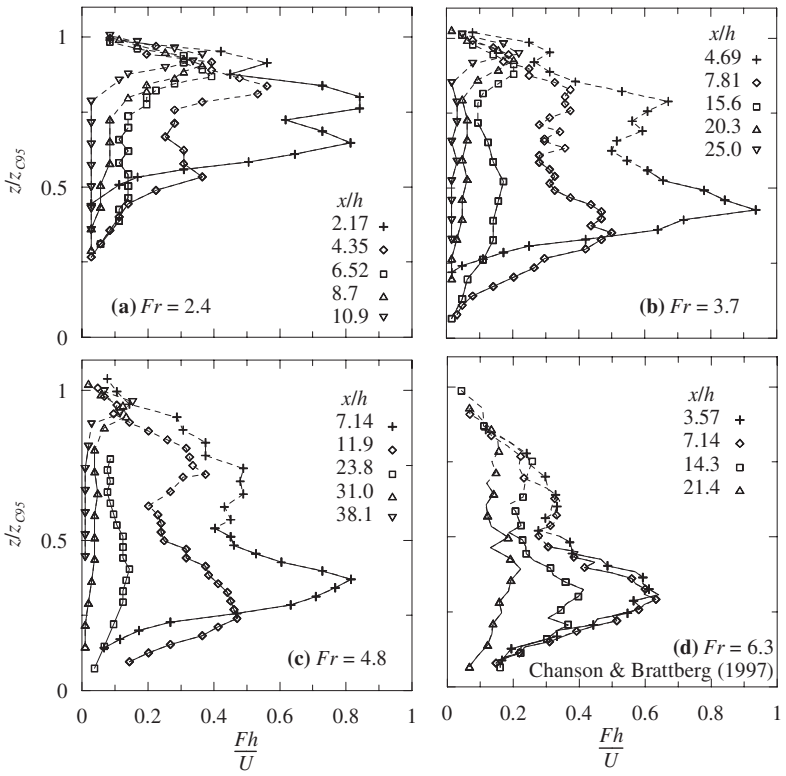

Fig. 9. Bubble frequencies as functions of elevation at various x. Continuous lines refer to the region $z < z^*$, broken lines to the region $z > z^*$.

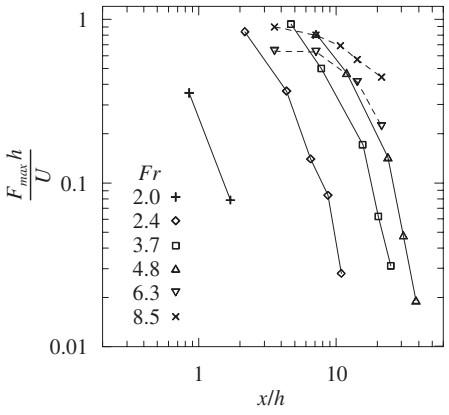

Fig. 10. Maximum bubble frequencies in the region $z < z^*$ as functions of distance downstream from the foot. Data for $Fr = 6.3$ and 8.5 (connected with broken lines) are from Chanson and Brattberg (1997).

above this elevation. These measurements are consistent with the image shown in Fig. 3, where the bubbles have an almost uniform size of around 4 mm over much of the water depth.

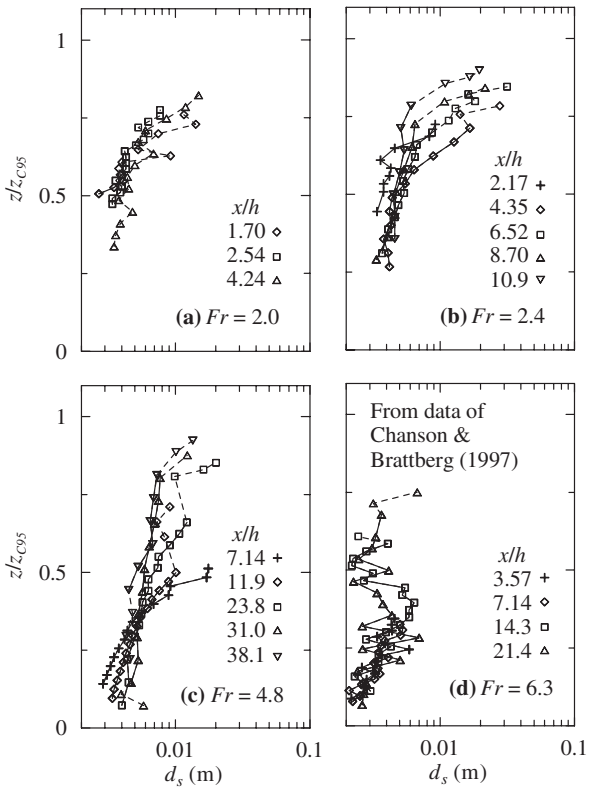

Fig. 11. Mean Sauter diameters plotted against elevation for different positions and Froude numbers in regions where $C < 0.25$. The elevations are normalised with respect to z_{C95} Continuous lines refer to the region $z < z^*$, broken lines to the region $z > z^*$.

4. Discussion and conclusions

Most previous measurements of aeration in hydraulic jumps have been made using conductivity probes, phase Doppler anemometry or acoustic Doppler velocimetry (which in certain conditions records the motion of bubbles). The main goal of the present work was to study the two-phase flow in a hydraulic jump by means of dual optical sensors, exploring new conditions and comparing our results with those in the literature. Our conclusions are as follows.

- In hydraulic jumps with Froude numbers between 2.0 and 8.5 (combining our results with those of Chanson and Brattberg (1997)) void fractions in the lower region, dominated by turbulent shear, followed a Gaussian distribution over a vertical profile (as suggested by Chanson (1996)). In the upper region, dominated by interfacial interactions, the data equally well followed a profile defined by an error function. The elevation of the interface between these zones could be clearly identified.
- In most respects, our results were consistent with the behaviour identified (at higher Froude numbers) by Chanson and Brattberg (1997, 2000). For example, excellent agreement was found

with their measurements of the elevation in the turbulent shear layer at which the void fraction reaches a maximum. On the other hand the maximum void fraction itself was generally found to fit better an exponential decay with distance along the flume, rather than a power law.

- There were also some notable differences in the distribution of bubble frequencies over the vertical. In our observations of the region close to the foot of the jump there was generally one maximum frequency within the turbulent shear layer, and another some distance above (though still well below the surface zone).
- For a convenient measure of the elevation of the upper surface of the jump we used that at which the void fraction reached 0.95. When Sauter mean diameters are scaled in this way they reveal a considerable degree of similarity over a wide range of Froude numbers and downstream positions.
- There is some evidence to suggest that at very high, and very low void fractions ($C < 0.02$), optical probes provide better quality data than conductivity probes. Our results appeared to be consistent down to $C \sim 0.001$ or better.

Continuing advances in instrumentation for measuring void fractions provide new opportunities for developing a better understanding of the interaction of strong turbulence with a free surface. The hydraulic jump is an attractive example of such a flow, though it involves air entrainment both from the foot of the jump and from violent interactions at the free surface. There remains considerable scope for further such measurements of the flow in hydraulic jumps, particularly on the effects of the upstream boundary layer and the quality of the water, and a need to relate the mechanisms of air entrainment to those that occur in other circumstances such as breaking waves, falling jets and turbulent wakes.

Acknowledgments

This work is supported by the EPSRC (contract GR/R85068) and through a European Community Marie Curie fellowship (contract HPMF-CT-2002-01897) held by the second author. The authors are grateful for discussions with D.H. Peregrine and D.C. Dunn, and thank H. Chanson for the provision of laboratory measurements.

References

Boyer, C., Duquenne, A.M., Wild, G., 2002. Measuring techniques in gas–liquid and gas–liquid–solid reactors. Chem. Eng. Sci. 57, 3185–3215.

Brattberg, T., Toombes, L., Chanson, H., 1998. Developing air–water shear layers of two-dimensional water jets discharging into air. In: Proc. FEDSM'98: ASME Fluids Engineering Division Summer Meeting, Washington DC.

Brocchini, M., Peregrine, D.H., 2001. The dynamics of strong turbulence at free surfaces. Part 1. Description. J. Fluid Mech. 449, 225–254.

Cartellier, A., Achard, J.L., 1990. Local phase detection probes in fluid/fluid two-phase flows. Rev. Sci. Instr. 62, 279–303.

Cartellier, A., Barrau, E., 1998. Monofiber optical probes for gas detection and gas velocity measurements: optimized sensing tips. Int. J. Multiphase Flow 24, 1295–1315.

Chanson, H., 1996. Air Bubble Entrainment in Free Surface Turbulent Flows. Academic Press.
Chanson, H., 1997. Air bubble entrainment in open channels: flow structure and bubble size distributions. Int. J. Multiphase Flow 23, 193–203.
Chanson, H., Brattberg, T., 1997. Experimental investigations of air bubble entrainment in developing shear layers. Report CH48/97, Department of Civil Engineering, University of Queensland, Australia.
Chanson, H., Brattberg, T., 2000. Experimental study of the air–water shear flow in a hydraulic jump. Int. J. Multiphase Flow 26, 583–607.
Chanson, H., Manasseh, R., 2003. Air entrainment processes in a circular plunging jet: void fraction and acoustic measurements. Trans. ASME: J. Fluids Eng. 125, 910–921.
Chanson, H, Qiao, G.L., 1994. Air bubble entrainment and gas transfer at hydraulic jumps. Research report CE149, Department of Civil Engineering, University of Queensland, Australia.
Clift, R., Grace, J.R., Weber, M.E., 1978. Bubbles, Drops and Particles. Academic Press, New York.
Liu, M., Zhu, D.Z., Rajaratnam, N., 2002. Evaluation of ADV measurements in bubbly two-phase flows. In: Hydraulic Proceedings of the Measurements and Experimental Methods Conference, ASCE, EWRI, Estes Park (CO), USA.
Mouaze, D., Murzyn, F., Chaplin, J.R., 2004. Turbulence at free surface in hydraulic jumps. In: Proc. HT FED 2004, ASME Heat Transfer/Fluids Engineering Conference.
Resch, F.J., Leutheusser, H.J., Coantic, M., 1976. Etude de la structure cinematique et dynamique du ressaut hydraulique. J. Hydraulic Res. 14, 293–319.
Waniewski, T.A., 2001. Bubble measurements downstream of hydraulic jumps. Int. J. Multiphase Flow 27, 1271–1284.
Wu, J., 2000. Bubbles produced by breaking waves in fresh and salt waters. J. Phys. Oceanogr. 30, 1809–1813.